Phase Change Materials in Buildings : Combined Optimisation of Melting-Peak Temperature and Melting Temperature Range.

Gilles Baudoin[1], Geoffrey van Moeseke[2]
[1,2]Architecture et Climat, Faculté d'architecture, d'ingénierie architecturale (LOCI)
Université Catholique de Louvain (UCL), 1 place du Levant, 1348 Louvain-la-Neuve, Belgium

Abstract

Phase Change Materials (PCMs) offer new opportunities to optimise thermal mass. The melting temperature is a key aspect of PCM selection, which can be characterised by the melting-peak temperature T_{mp} and the melting temperature range ΔT_{m}. While T_{mp} has been studied extensively, little research has focused on ΔT_{m}. This study investigates the optimal combination (T_{mp}, ΔT_{m}) by simulating a test-cell based on a nearly zero-energy office building in a temperate climate. Our results show that the optimal T_{mp} varies slightly with ΔT_{m} for heating and cooling energy demand indicators while aggregated indicators can be more influenced by ΔT_{m}.

Introduction

PCMs allow to increase the thermal mass effect on a given temperature range. For this reason, researchers have shown an increased interest in PCM to optimise thermal mass in the building sector (see the review articles of Soares et al. (2013) and Kalnæs and Jelle (2015)).

The potential effect of PCMs can be strongly affected by its properties and building parameters. The three main properties of a quasi-ideal PCM are the melting-peak temperature T_{mp}, the melting temperature range ΔT_{m} and the latent heat E_{l} (Figure 1). An ideal solid-liquid PCM would melt and solidify at T_{mp} and the latent heat would be stored and released at this temperature.

This article explores the optimal melting-peak temperature T_{mp} and melting temperature range ΔT_{m} of a quasi-ideal PCM in terms of energy demand and comfort, for the Belgian climate.

Melting-peak temperature selection T_{mp} has been studied in different climates either by the proper choice of available commercial products or more systematically by modelling theoretical PCMs. However, little research has focused on the melting temperature range ΔT_{m} (Table 1).

The setpoint temperature T_{th} can be one of the key building parameters for PCM selection. The influence of T_{th} on T_{mp} has been studied by Soares et al. (2017). This study has been focused on the cooling load with a ΔT_{m} fixed at 4.0 °C for the Kuwait climate.

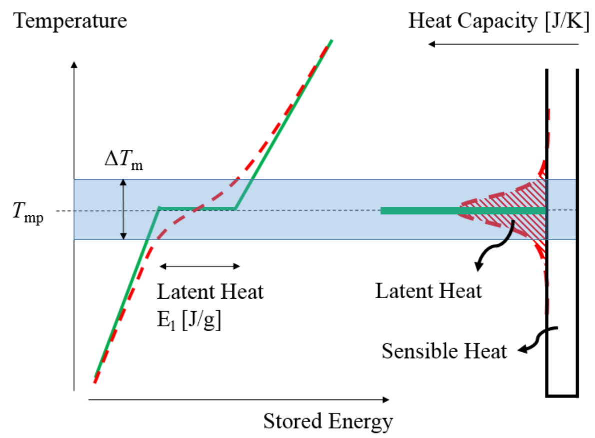

Figure 1: PCMs properties in the Enthalpy/Temperature curve and the associated heat capacity. Ideal behaviour (green) and quasi-ideal behaviour (red dotted line).

The Key Performance Indicators (KPIs) vary in the different studies concerning PCM selection. In some cases, an air-conditioned test-cell is considered and in other cases, a free-running building. In this work, both approaches were taken into consideration.

The present work aims at evaluating the optimum (T_{mp}, ΔT_{m}) combination and to evaluate the sensitivity of this result to T_{th} and the choice of KPI. This is done through the simulation of a typical test-cell commonly used in similar studies, adapted to the Belgian context for a nearly zero-energy expected performance office building.

Table 1: Literature summary of parameters range T_{mp} and ΔT_{m} in dynamic building simulations.

Reference	T_{mp} [°C]	ΔT_{m} [°C]
Evola et al. (2013)	23.6 - 28.6 by 1	6.5
Soares et al. (2014)	18 - 28 by 2	8
Alam et al. (2014)	20 - 25 by 1	4
Saffari et al. (2016)	23 - 27 by 2	4
Lei et al. (2016)	22 - 32 by 1	0.1, 4
Soares et al. (2017)	18 - 30 by 2	8
Saffari et al. (2017)	20 - 26 by 0.01	4

Method

Annual dynamic building simulations were realised for a simplified test-cell based on a highly efficient office building, using EnergyPlus 8.8.0 (Table 2). After defining a base case with a 2cm-thick PCM-panel without phase change properties, with an exchange surface of 1 m^2/m^2 of floor area, PCM properties were added to this PCM-panel. This allowed to dissociate latent from sensible heat effect. The latent heat was fixed based on common value found in the literature and the variables, T_{mp} and ΔT_m, varied according to the range given in table 2. After calculating KPIs for every 363 (T_{mp}, ΔT_m) couples, a 3D graph and the associated contour plot were built. To evaluate the influence of T_{th}, 3 cross-sections of the 3D plot were taken at $\Delta T_m = 0.1$, 5 and 10 °C.

Test-cell

The test-cell dimensions were based on the model specified in ASHRAE (2007) 140 standard (Figure 2). The orientation of the windows was arbitrary set to the north as a starting point for further investigations.

The north-oriented surface had outdoor boundary condition and the other surfaces were defined as internal surfaces with an adiabatic boundary condition. The details about envelope composition and test-cell loads can be found in the appendix.

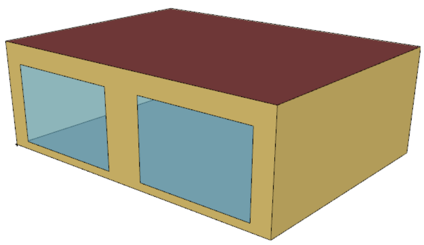

Figure 2: Test-cell based on ASHRAE Standard 140.

Heat recovery system, diurnal and night freecooling were implemented in a simplified way using the IdealLoadsAirSystem object in EnergyPlus. The enthalpic heat recovery had a sensible effectiveness of 79% and a latent effectiveness of 77%. The freecooling was based on difference in air dry bulb temperature and the outside air flow was allowed to increase up to 2 Air Changes per Hour (ACH). For nightcooling, the cooling load calculation was based on the same T_{th} than the diurnal temperature control. In order to be able to limit the freecooling flow rate, two IdealLoadsAirSystem objects were used. The limit on the freecooling flow rate would indeed apply to the ideal air load supply air and would not allow to achieve the necessary cooling load.

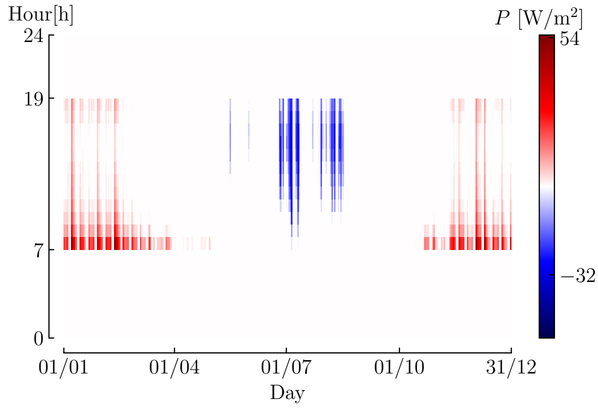

Figure 3: Hourly power loads for the base case (Category II) with the ideal HVAC system.

This base case had annual heating energy needs of 5.11 kWh/m^2 and annual cooling energy needs of 3.35 kWh/m^2, which were both below the passive house criteria of 15.0 kWh/m^2 (Passive House Institute (2016)). The distribution of power loads varied between heating and cooling (Figure 3). While high power needs were required at the beginning of the day for heating, more constant needs were generally required in the afternoon for the cooling.

PCMs simulation

A PCM-panel with a width of 2 cm and a exchange surface of 1 m^2/m^2_{floor} was added as an internal mass object in the test-cell. This approach allowed to consider the addition of PCM properties regardless of its position in the test-cell. The PCM-panel was directly in contact with the inside environment. For the base case, no phase change properties were used for this PCM-panel.

The PCM-panel properties were based on data used

Table 2: Case descriptions in this parametric study.

Study cases	T_{mp} [°C]	ΔT_m [°C]	Regulation	Thermal comfort
Base case	No PCM effect	No PCM effect	Air-conditioning	Category II
Base case free-running	No PCM effect	No PCM effect	Free-running	Category II
Influence of T_{mp} and ΔT_m	14 - 30 by 0.5	0.1, 1 - 10 by 1	Air-conditioning	Category II
Influence of T_{th}	14 - 30 by 0.5	0.1, 5 and 10	Air-conditioning	Category I-II-III
Influence of KPI	14 - 30 by 0.5	0.1, 1 - 10 by 1	Free-running	Category II
Influence of adaptive theory	14 - 30 by 0.5	0.1, 1 - 10 by 1	Free-running	Adaptive category II

by Tabares-Velasco et al. (2012), which referred to DuPont Energain PCM. This product comes as an aluminium-laminated panels which contain a copolymer and paraffin wax compound. The latent heat is 110 kJ/kg , the density 855 kg/m^3 and the specific heat 2500 J/kgK. In this work the thermal conductivity value was assumed not to vary between the solid and liquid phase, and fixed to 0.16 W/mK.

The PCM behaviour was considered as quasi-ideal i.e. no hysteresis, nor sub-cooling effects were taken into account. The EnergyPlus PCM model developed by Tabares-Velasco et al. (2012) was used with a timestep of 3 minutes and a space discretization constant of 3.

The sensible heat of the PCM-panel was about 21 kJ/Km^2 and the additional thermal energy storage due to the PCM latent heat was about 940 kJ/m^2 (261 Wh/m^2). The main field of investigation was to know how to distribute this additional storage capacity in terms of T_{mp} and ΔT_{m}.

The apparent heat capacity was modelled as a normal curve centred in T_{mp}. The standard deviation σ was linked to ΔT_{m} by $\sigma = \Delta T_{\mathrm{m}}/4$. Based on this apparent heat capacity, the enthalpy/temperature curve was numerically built, respecting the relationship $C_{\mathrm{app}}(T) = \frac{\delta E(T)}{\delta T}$. Then, 15 (T, E) points were selected as input for the Energy Plus PCM model. The first point was taken at -20 °C and the last one at 100 °C. The others were evenly spaced from $T_{\mathrm{mp}} - 3\sigma$ to $T_{\mathrm{mp}} + 3\sigma$.

Weather data

The weather data used came from the International Weather for Energy Calculation (IWEC) data file (ASHRAE (2001)), which is a typical weather file for building energy simulation for Uccle in Belgium.

The climate is classified as Cfb according to the Köppen-Geiger climate classification, such as a major part of the Northwest Europe weather.

Key performance indicators

KPIs were different for the two main approaches, which were the air-conditioning, with heating and cooling setpoint temperature, and the free-running temperature approach.

In the air-conditioned case, the ideal air load template was used. It allowed to get the cooling energy E_{cool} that the cooling system had to remove and the heating energy E_{heat} that the heating system had to provide. It was independent of a cooling and heating system efficiency. The setpoint temperature T_{th} was based on the operative temperature T_{op} defined according to comfort categories from Standard EN 15251 (European Committee for Standardization (2007)) (Table 4). The total energy E_{tot} was defined as the sum of E_{cool} and E_{heat}, as it had already been done in similar studies on PCMs (e.g. Soares et al. (2014)). These indicators were normalised by m^2 of floor area.

Table 4: T_{op} based on comfort categories from Standard EN 15251

Comfort category	T_{op} for heating [°C]	T_{op} for cooling [°C]
Cat I	21.0	25.5
Cat II	20.0	26.0
Cat III	19.0	27.0

In the free-running temperature case, the heating and cooling system availability schedules were defined as always OFF. The indicator Intensity of Thermal Discomfort (ITD) was used as described by Evola et al. (2013) and in the appendix F of Standard EN 15251. ITD_{cool} is the time integral over the occupancy period of the difference of the current T_{op} and the maximum T_{op} for cooling of a given comfort category (Table 4) for $T_{\mathrm{op}} > T_{\mathrm{op}}$ for cooling. A similar definition is given for ITD_{heat}. As for E_{tot}, a ITD_{tot} was defined as the sum of ITD_{cool} and ITD_{heat}.

To consider the adaptive theory for cooling, the T_{op} threshold for cooling was defined as described in the appendix A.2 to vary in function of the external temperature. The associated $ITD_{\mathrm{cool,adapt}}$ was then calculated with this variable T_{op} threshold.

The savings due to PCM properties compared to the base case were written as ΔE and ΔITD.

Table 3: Main results in terms of energy demand and thermal comfort (Category II) with the optimal ($T_{\mathrm{mp}}{}^*$, $\Delta T_{\mathrm{m}}{}^*$) and the associated savings compared to the base case.

KPI to minimise	Base case [kWh/m^2] or [Kh]	$T_{\mathrm{mp}}{}^*$ [°C]	$\Delta T_{\mathrm{m}}{}^*$ [°C]	Savings [kWh/m^2] or [Kh]	Relative savings [%]
E_{cool}	3.35	25.0	0.1	1.45	43
E_{heat}	5.11	19.5	0.1	1.13	22
E_{tot}	8.46	25.0	0.1	1.45	17
ITD_{cool}	398.29	25.5	1.0	187.94	47
ITD_{heat}	2354.89	19.0	0.1	652.36	27
ITD_{tot}	2753.18	19.0	0.1	652.42	23
$ITD_{\mathrm{cool,adapt}}$	53.42	26.0	2.0	48.40	90

Results and discussion

Air-conditioning case

The incorporation of the optimal $T_{mp}{}^*$ and $\Delta T_m{}^*$ for cooling and heating results in savings, which were higher for cooling (1.45 kWh/m^2) than for heating (1.13 kWh/m^2) in absolute and relative values (Table 3). Even though these results were not directly comparable with previous studies due to different building system hypothesis and PCM properties, they were relatively low compared with similar studies for Cfb climates. In the Paris climate, Soares et al. (2014) obtained a base case E_{cool} of 14.21 kWh/m^2 and E_{cool} with PCM of 4.02 kWh/m^2, resulting in 10.18 kWh/m^2 savings. For heating, they obtained a base case E_{heat} of 30.67 kWh/m^2 and E_{heat} with PCM of 24.77 kWh/m^2, resulting in 5.90 kWh/m^2 savings. Alam et al. (2014) achieved savings of the order of 20 kWh/m^2 and Saffari et al. (2017), considering the HVAC system efficiency of a typical office building and with less PCM quantity, achieved savings of the order of less than 1 kWh/m^2 for the Paris climate.

Concerning the optimal $T_{mp}{}^*$, the optimal value for heating $T_{mp}{}^*$ 19.5 °C was just below the T_{op} for heat-

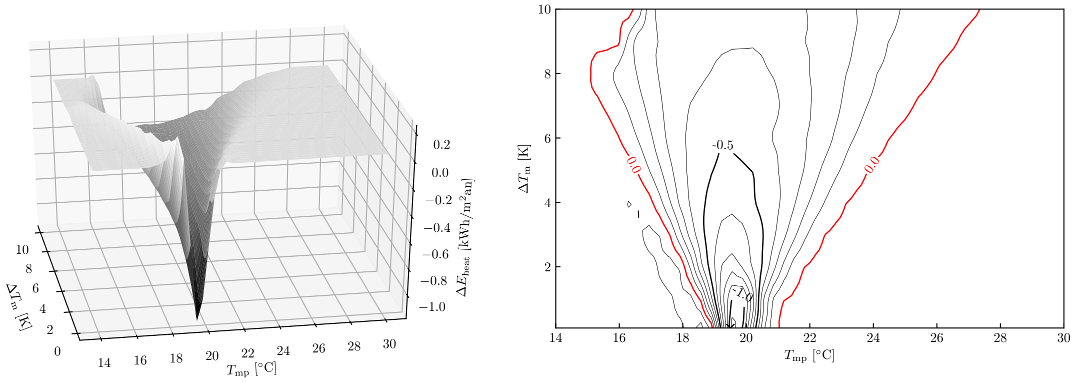

(a) Annual heating energy.

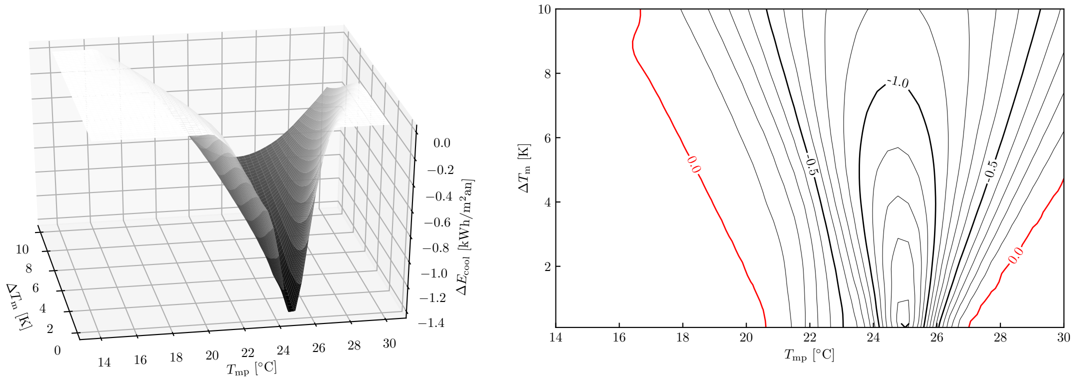

(b) Annual cooling energy.

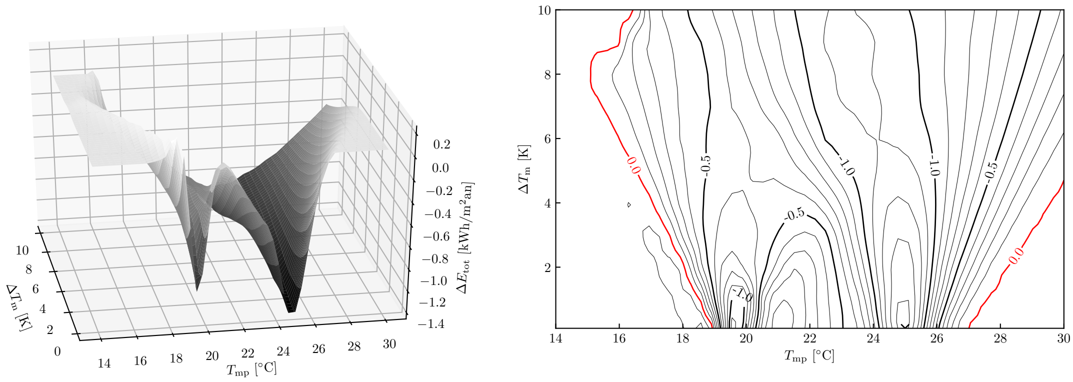

(c) Annual total energy.

Figure 4: Air-conditioning approach (Comfort category II): influence of T_{mp} and ΔT_m on annual energy demand. The cross is placed at ($T_{mp}{}^*$, $\Delta T_m{}^*$), the optimal value that maximises the effect of the PCM.

ing 20.0 °C. For cooling, T_{mp}* 25.0 °C was more spaced from the T_{op} for cooling 26.0 °C. Considering E_{tot}, the optimal value T_{mp}* was also 25.0 °C, which differed from what Soares et al. (2014) obtained, a value of 22.0 °C for the major part of the PCM added to the test-cell. This comparison has to be taken cautiously because, unlike the present study, thermostat was based on inside air temperature with heating and cooling threshold of 20.0 and 25.0 °C. Similarly, Alam et al. (2014) obtained an optimal T_{mp}* of 21.0 °C with heating and cooling threshold of 20.0 and 24.0 °C. Saffari et al. (2017) obtained 25.13 °C for E_{cool}, 24.06 °C for E_{heat} and 24.06 °C for E_{tot} with heating and cooling T_{op} threshold of 20.0 and 26.0 °C.

For the optimal T_{mp}, the increase of ΔT_m had a more negative effect on heating (Figure 4a) than on cooling (Figure 4b). For example, the saving on E_{cool} decreased from 1.45 (ΔT_m = 0.1) to 0.93 kWh/m^2 by changing ΔT_m from 0.1 to 10.0 °C. It corresponded to a decrease of the effect of the PCM of 0.52 kWh/m^2 (36%). The saving on E_{heat} decreased from 1.13 to 0.38 kWh/m^2 by changing ΔT_m from 0.1 to 10.0 °C. It corresponded to a decrease of the effect of the PCM of 0.75 kWh/m^2 (66%).

T_{mp} optimal varied slightly with ΔT_m. For heating, it increased from 19.5 to 20.5 °C (ΔT_m=9.0 °C) and decreased to 18.5 °C (ΔT_m=10.0 °C). For cooling, it decreased from 25.0 to 24.5 °C. When ΔT_m increased, the energy savings were less sensitive to a non-optimal selection of T_{mp}. The contour lines were indeed more spaced near the optimal T_{mp} for each ΔT_m with increasing ΔT_m. It is worth noting that a non-optimal selection of T_{mp} with low ΔT_m would affect more the savings for heating than for cooling. Our results suggest that the optimum T_{mp} could be approached independently of ΔT_m if the required accuracy on T_{mp} is less than 1.0 °C.

Concerning the optimal T_{mp} for E_{tot}, more caution should be taken to estimate the optimal T_{mp} (Figure 4c). For example, a ΔT_m of 4.0 °C would lead to a selection of T_{mp} of 25.0 °C, while a ΔT_m of 9.0 °C would lead to a selection of T_{mp} of 23.0 °C.

The addition of PCM properties led to a decrease or had no effect on the cooling energy requirement for every couples of (T_{mp}, ΔT_m) tested (Figure 4b). On the contrary, some parts of the (T_{mp}, ΔT_m) combination led to an increase of energy requirement for heating that could reach 0.2 kWh/m^2 (Figure 4a).

Influence of the thermostat setpoint temperature

The optimal T_{mp}* varied in function of T_{th} (Figure 5). In the case of cooling, T_{mp}* was situated at T_{th} -1.5 or -1.0 °C for ΔT_m = 0.1 °C and at T_{th} -0.5 °C in the heating case. When ΔT_m increased, the optimal T_{mp}* varied only in the order of 0.5, 1.0 °C for the three different T_{th}.

Besides, two interesting facts could be observed on fig. 5. Firstly, the energy savings for cooling due to the integration of PCM were more affected by different T_{th} than the savings for heating.

Secondly, the heating cases were more sensitive to a wrong choice of T_{mp} and to a change of T_{th}. For example, the best result for the T_{th} based on Cat II would lead to negative effect for T_{th} based on Cat I in the case of ΔT_m = 0.01 °C.

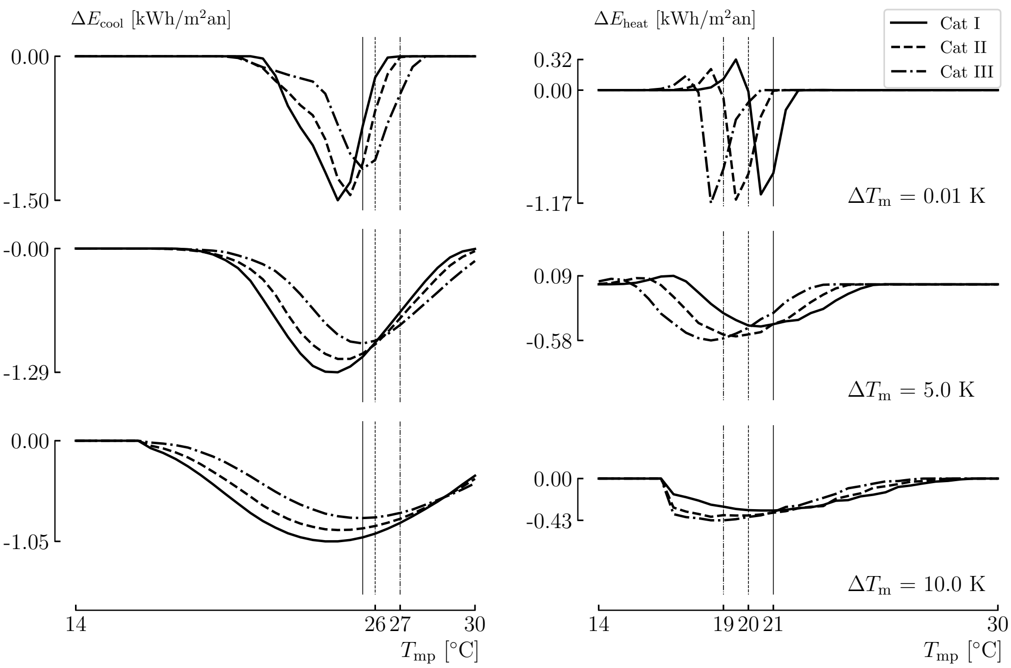

Figure 5: Annual cooling (left) and heating (right) energy savings in function of T_{mp} for three different thermostat setpoint temperatures (Cat I-II-III) and 3 different ΔT_m.

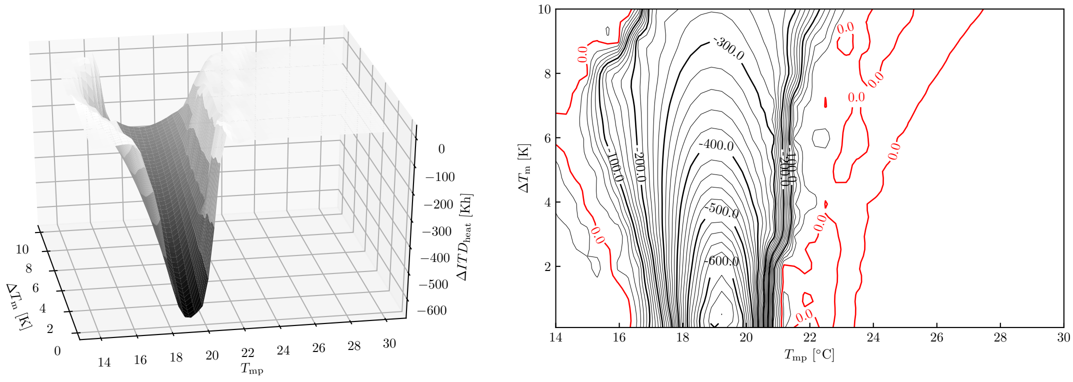

(a) ITD heating.

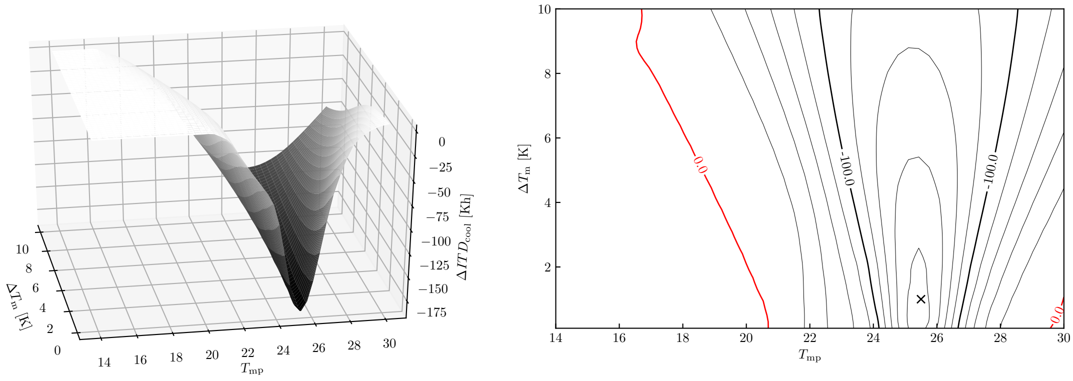

(b) ITD cooling.

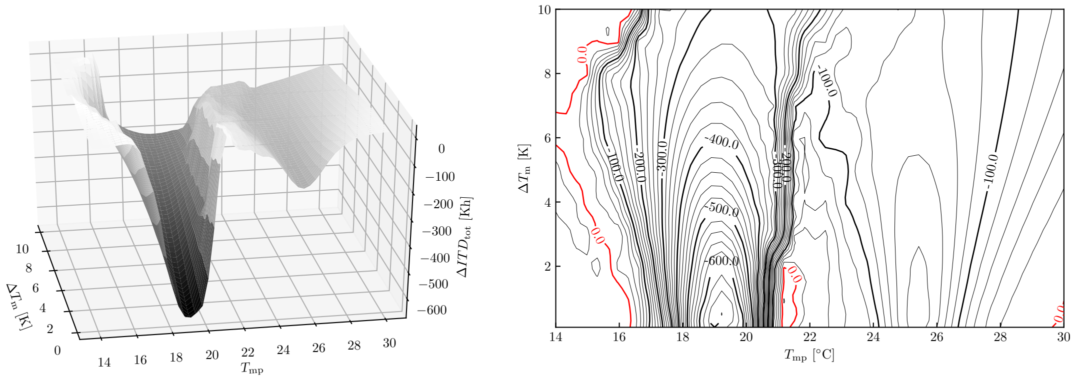

(c) ITD total.

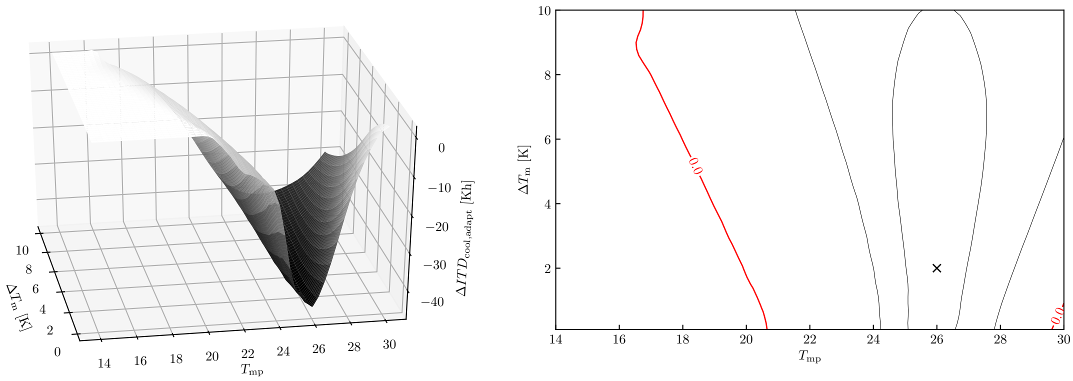

(d) ITD for cooling with respect to adaptive comfort limit.

Figure 6: Free-running approach (Comfort category II): influence of T_{mp} and ΔT_m on ITD indicator. The cross is placed at ($T_{mp}{}^*$, $\Delta T_m{}^*$), the optimal value that maximises the effect of the PCM.

Free-running case

In the free-running case with ITD_{heat} and ITD_{cool} as KPI, the optimal combination ($T_{\mathrm{mp}}{}^*$, $\Delta T_{\mathrm{m}}{}^*$) was similar to the air-conditioning case with E_{heat} and E_{cool} as KPI. $T_{\mathrm{mp}}{}^*$ differed by 0.5 °C and $\Delta T_{\mathrm{m}}{}^*$ differed by 0.9 °C, only in the cooling case. Concerning the aggregated indicators ITD_{tot} and E_{tot}, the $T_{\mathrm{mp}}{}^*$ for ITD_{tot} differed by 6.0 °C (Table 3).

In the free-running case, ITD_{heat} had a more important part in ITD_{tot} (86%) than E_{heat} in E_{tot} (60%). The ITD_{heat} contour map (Figure 6a) had got different heating summit position and the space with positive effect varied compared to the E_{heat} case. The main difference in ITD_{cool} graph (Figure 6b) and E_{cool} was the fact that the zone of positive PCM effect extended for higher T_{mp}. The ITD_{tot} graph (Figure 6c) showed similar trends.

Adaptive comfort

$ITD_{\mathrm{cool,adapt}}$ was less important than ITD_{cool} (Table 3). Even tough absolute savings were less important for $ITD_{\mathrm{cool,adapt}}$ than for ITD_{cool}, relative savings were higher, 90% compared to 47%. In terms of T_{mp} and ΔT_{m}, the optimal values for $ITD_{\mathrm{cool,adapt}}$ were slightly higher, 26.0 compared to 25.5 °C and 2.0 compared to 1.0 °C. The contour lines were also more spaced, resulting in less sensitivity to a less optimal T_{mp} and ΔT_{m} selection (Figure 6d).

Simulating a test-cell with the Chambery climate (France), Evola et al. (2013) achieved less relative savings of the order of 31.2% for $ITD_{\mathrm{cool,adapt}}$ and an associated $T_{\mathrm{mp}}{}^*$ of 26.6 °C based on a thermostat threshold of category I.

Conclusion

This paper has investigated the optimal combination of melting-peak temperature and melting temperature range (T_{mp}, ΔT_{m}) by simulating a test-cell based on a nearly zero-energy office building in the Belgian climate.

The optimal T_{mp} varied slightly with ΔT_{m}, i.e. of the order of less than 1.0 °C, with ΔT_{m} from 0.1 to 10.0 °C. This small variation was observed for both the air-conditioning case, with three different thermostat setpoint temperatures, and for the free-running case. Meanwhile, the aggregated indicator E_{tot} was an exception with a variation that could reach 2.0 °C.

The optimal T_{mp} could be outside the comfort temperature range for low ΔT_{m} in the heating case. This phenomenon was not explained and was probably linked to the dynamic temperature patterns of heating season, which are characterised by temperature falling during the night and high energy demand at the beginning of the day.

In the air-conditioning case, the addition of PCM properties led to more savings, in absolute and relative values, for cooling than for the heating case, which was more sensitive to a non-optimal selection of T_{mp} and to an increase of ΔT_{m}. Some combinations of T_{mp} and ΔT_{m} even led to an increase of energy demand or thermal discomfort for the heating case. In the free-running case, the savings were higher for the heating case, which led to the same PCM selection for ITD_{tot} and ITD_{heat}.

The findings presented here provide a starting point for further examination of the influence of other parameters on the optimum (T_{mp}, ΔT_{m}) selection. These parameters could include those related to PCMs such as latent energy E_{l} and hysteresis effect, those related to PCM-enhanced product such as location, quantity and exchange surface and those related to building system properties such as design, operational and external conditions.

Appendix

Test-cell envelope

The test-cell was modelled thanks to the OpenStudio Plugin in Sketchup 2017. The surface compositions are given in table 5. The external wall was based on the ASHRAE 140 standard model with an increase of insulation thickness in order to achieve the belgian regulation of a U-value below 0.24 W/m^{2}K. For the other internal surfaces, the composition was based on a typical office building in Belgium and the material properties were given by the Belgian regulation (Gourvernement wallon (2017)). The windows were considered using the simple glazing system model. The whole window component was characterised by a U-value of 1.5 W/m^{2}K, a Solar Heat Gain Coefficient of 0.62 and a visible transmittance of 0.70. For the convective heat transfer of inside surfaces, the default algorithm TARP in EnergyPlus was used. The influence of the algorithm used is subject to further inverstigations.

Test-cell loads details

The occupancy load depended on the number of people 0.07 person/m^2 and a constant metabolic rate of 110 W/person. It gave an occupancy load of 7.7 W/m^2. This load was modulated by the occupancy schedule 25% between 7:00 and 8:00, 50% between 8:00 and 9:00, 100% between 9:00 and 12:00, 75% between 12:00 and 14:00, 100% between 14:00 and 17:00, 50% between 17:00 and 18:00 and 25% between 18:00 and 19:00. The room was considered occupied only within weekdays and occupancy hours.

The maximum equipment load was 6 W/m^2 with 100% between 7 and 19 hours and 0.05% the rest of the day and the weekends. The maximum lighting load was 4 W/m^2 with 100% between 7 and 19 hours and 0% the rest of the day and the weekends.

The ventilation rate was fixed at 0.00101 m^3/m$^2_{\mathrm{floor}}$s (3.636 m^3/m$^2_{\mathrm{floor}}$h) with 100% between 7 and 19 hours and 0% the rest of the day and the weekends, and the infiltration rate was fixed at 0.03 ACH.

Table 5: Test-cell envelope composition.

		Thickness [m]	λ [W/mK]	Density [kg/m^3]	Specific heat [kJ/kgK]
Internal floor/ceiling	Carpet	0.008	0.06	200	1300
	Cement screed	0.06	0.93	1900	1000
	Reinforced concrete	0.04	1.7	2400	1000
	Precast concrete slab	0.16	1.23	1870	1000
	Plaster	0.01	0.52	1300	1000
Internal wall	Plasterboard	0.012	0.35	900	1000
	Mineral Wool	0.06	0.05	35	1030
	Plasterboard	0.012	0.35	900	1000
External wall	Wood siding-1	0.009	0.14	530	900
	Fiberglass quilt-1	0.16	0.04	12	840
	Plasterboard-1	0.012	0.16	950	840

Acknowledgement

FEDER (le Fonds européen de développement régional) and Wallonia have funded this research project in the framework of operational programme Wallonie-2020.EU.

References

Alam, M., H. Jamil, J. Sanjayan, and J. Wilson (2014). Energy saving potential of phase change materials in major Australian cities. *Energy and Buildings 78*, 192–201.

ASHRAE (2001). International Weather for Energy Calculations (IWEC weather files) users manual and CD-ROM.

ASHRAE (2007). Standard 140 - standard method of test for the evaluation of building energy analysis computer programs.

European Committee for Standardization (2007). CEN Standard EN 15251: Indoor environmental input parameters for design and assessment of energy performance of buildings addressing indoor air quality, thermal environment, lighting and acoustics.

Evola, G., L. Marletta, and F. Sicurella (2013). A methodology for investigating the effectiveness of PCM wallboards for summer thermal comfort in buildings. *Building and Environment 59*, 517–527.

Gourvernement wallon (2017). Annexe B1 DRT - Règle pour le calcul des pertes par transmission dans le cadre de la réglementation PEB.

Kalnæs, S. E. and B. P. Jelle (2015). Phase change materials and products for building applications: A state-of-the-art review and future research opportunities. *Energy and Buildings 94*, 150–176.

Lei, J., J. Yang, and E.-H. Yang (2016). Energy performance of building envelopes integrated with phase change materials for cooling load reduction in tropical Singapore. *Applied Energy 162*, 207–217.

Passive House Institute (2016). Criteria for the Passive House, EnerPHit and PHI Low Energy Building Standard.

Saffari, M., A. de Gracia, C. Fernndez, and L. F. Cabeza (2017). Simulation-based optimization of PCM melting temperature to improve the energy performance in buildings. *Applied Energy 202*, 420–434.

Saffari, M., A. de Gracia, S. Ushak, and L. F. Cabeza (2016). Economic impact of integrating PCM as passive system in buildings using Fanger comfort model. *Energy and Buildings 112*, 159–172.

Soares, N., J. J. Costa, A. R. Gaspar, and P. Santos (2013). Review of passive PCM latent heat thermal energy storage systems towards buildings energy efficiency. *Energy and Buildings 59*, 82–103.

Soares, N., A. R. Gaspar, P. Santos, and J. J. Costa (2014). Multi-dimensional optimization of the incorporation of PCM-drywalls in lightweight steel-framed residential buildings in different climates. *Energy and Buildings 70*, 411–421.

Soares, N., C. F. Reinhart, and A. Hajiah (2017). Simulation-based analysis of the use of PCM-wallboards to reduce cooling energy demand and peak-loads in low-rise residential heavyweight buildings in Kuwait. *Building Simulation*, 1–15.

Tabares-Velasco, P. C., C. Christensen, and M. Bianchi (2012). Verification and validation of EnergyPlus phase change material model for opaque wall assemblies. *Building and Environment 54*, 186–196.